Layered acoustofluidic resonators for the simultaneous optical and acoustic characterisation of cavitation dynamics, microstreaming, and biological effects

V. Pereno,[1,a)] M. Aron,[1,a)] O. Vince,[1] C. Mannaris,[1] A. Seth,[1] M. de Saint Victor,[1] G. Lajoinie,[2] M. Versluis,[2] C. Coussios,[1] D. Carugo,[1,3,b)] and E. Stride[1,b)]

[1]*Department of Engineering Science, Institute of Biomedical Engineering, University of Oxford, Oxford OX3 7DQ, United Kingdom*
[2]*Physics of Fluids Group, MESA+ Institute for Nanotechnology and MIRA Institute for Biomedical Technology and Technical Medicine, University of Twente, P.O. Box 217, 7500 AE Enschede, The Netherlands*
[3]*Department of Mechanical Engineering, Faculty of Engineering and the Environment, University of Southampton, Southampton SO17 1BJ, United Kingdom*

The study of the effects of ultrasound-induced acoustic cavitation on biological structures is an active field in biomedical research. Of particular interest for therapeutic applications is the ability of oscillating microbubbles to promote both cellular and tissue membrane permeabilisation and to improve the distribution of therapeutic agents in tissue through extravasation and convective transport. The mechanisms that underpin the interaction between cavitating agents and tissues are, however, still poorly understood. One challenge is the practical difficulty involved in performing optical microscopy and acoustic emissions monitoring simultaneously in a biologically compatible environment. Here we present and characterise a microfluidic layered acoustic resonator (μLAR) developed for simultaneous ultrasound exposure, acoustic emissions monitoring, and microscopy of biological samples. The μLAR facilitates *in vitro* ultrasound experiments in which measurements of microbubble dynamics, microstreaming velocity fields, acoustic emissions, and cell-microbubble interactions can be performed simultaneously. The device and analyses presented provide a means of performing mechanistic *in vitro* studies that may benefit the design of predictable and effective cavitation-based ultrasound treatments. *Published by AIP Publishing.* https://doi.org/10.1063/1.5023729

I. INTRODUCTION

A. Cavitation in ultrasound (US) therapy

Over the past three decades, the potential of ultrasound (US) to increase the permeability of biological membranes to different classes of therapeutically active compounds has been widely demonstrated, paving the way for its use in the treatment of malignant and non-malignant diseases.[1–3] Cavitation, the creation and subsequent oscillation of gas and/or vapour bubbles, has been shown to play a key role in this process.[4] Consequently, a variety of different ultrasound-responsive agents (US-RAs), including coated gas microbubbles, phase-shift nanodroplets, and gas entrapping solid nanoparticles,[5–7] have been developed to promote cavitation and thus enhance or localise the mechanical perturbation induced by US alone. The systemic distribution, circulation time, and acoustic responsiveness of these agents strongly depend on both the physical properties (i.e., size, compressibility, density) of the particles and the

---

a)V. Pereno and M. Aron contributed equally to this work.
b)Authors to whom correspondence should be addressed: d.carugo@soton.ac.uk and eleanor.stride@eng.ox.ac.uk

chemical composition and charge of the surface coating. These properties can potentially be tailored for a desired application or therapeutic outcome. Moreover, agents can be functionalised with targeting species for efficient accumulation at a specific organ or tissue, upon application of external physical stimuli (e.g., magnetic fields[8]) or *via* bio-chemical interactions.[9]

Performance optimisation and clinical translation of US-RAs, however, require a comprehensive understanding of the mechanisms of interaction with biological systems, from the sub-cellular level upwards. These mechanisms include a range of phenomena:[10] direct interaction between bubbles and cells through impingement[11] disrupting the cell membrane or activating mechanosensitive ion channels; the production of microjets during bubble collapse[12] perforating the cell membrane; material transfer[13,14] altering the physical properties of the membrane; production of chemical species such as hydrogen peroxide;[15] shockwaves emitted by collapsing bubbles, and cavitation induced microstreaming, which may facilitate drug delivery by increasing transport and mixing and/or by imposing high levels of shear stress and spatial and/or temporal shear stress gradients.[16–18] The diversity of these mechanisms makes their study extremely challenging, as does the range of time and lengthscales over which they operate, from nanoseconds to hours and from sub-nanometre to mm, respectively. A detailed review of the techniques that have been applied and/or developed for this purpose may be found in Ref. 19. Section I B provides a brief overview.

B. Existing devices

Advanced analytical and optical instruments have been developed to probe the physical and chemical properties of biological cells and sub-cellular structures, at increasingly high spatial and temporal resolution.[13,20–23] The integration of commercial analytical and optical instrumentation with custom-built ultrasound stimulation rigs (i.e., water-tank based apparatus) however poses significant practical and technical challenges.[19] A typical experimental setup for ultrasound-mediated stimulation of biological samples consists of an acoustically and optically transparent chamber, such as an Opticell[TM] (Refs. 13 and 24) (Thermo Fisher Scientific) or other custom-built devices.[25] These chambers are biologically compatible and suitable for the generation of a well-defined and clinically relevant acoustic field. To do so however requires the use of a relatively large volume water tank, which limits the degree to which they can be integrated with optical microscopy systems. Moreover, parallel-plate chambers are often not designed for continuous-flow experimentation and may suffer from high wall shear stress during priming or practical difficulties in removing exogenous air bubbles.[25]

Alternative devices that do not require immersion in a water tank have been employed to investigate the physical and/or biological effects of cavitating agents. These include glass cuvettes, capillaries, and cylindrical chambers that can be coupled to a piezoelectric (PZT) element.[26,27] Given their material and dimensional properties, acoustic standing waves may compromise the uniformity of the acoustic pressure field, and devices are often not suitable for high-resolution microscopy or for performing biological assays. Moreover, they are typically driven at relatively low ultrasound frequencies (i.e., 20–200 kHz) compared to the MHz range of frequencies used in therapeutic applications.

Microfluidic devices with integrated ultrasound sources (either bulk or surface waves) have also been reported, providing the advantage of physiologically relevant confinement and optical imaging at high spatial resolution.[28–30] They have been employed to investigate the behaviour of gas microbubbles under US excitation or to elicit membrane permeabilisation, but are often actuated at relatively high US frequencies (i.e., ≥ 2 MHz) corresponding to a resonance frequency of a composite structure and that are not therapeutically relevant. Moreover, the acoustic pressure in these systems is typically below the therapeutically relevant range, and strongly resonating structures may suffer from large acoustic pressure amplitude gradients in the internal fluid cavity. Such devices are also not typically reusable, and their inner surfaces are difficult to treat or coat, if the constitutive layers are permanently bonded together (i.e., *via* treatment with oxygen plasma).

More conventional "acoustofluidic" devices utilise ultrasound standing wave (USW) fields within a fluid cavity in order to manipulate microparticles, biological cells, or microorganisms towards specific regions of the ultrasound field.[31,32] These usually correspond to the pressure nodes of the USW, the positions of which can be tuned on-demand to achieve cell separation and sorting, sample filtration and concentration, or detection of target cells/organisms.[33] Notably, acoustofluidic devices have also been employed to investigate the enhanced mixing of chemical species associated with flow perturbations from cavitating microbubbles.[34–39] Acoustofluidic devices designed for acoustic manipulation normally comprise strong acoustic pressure and energy density gradients within their fluid cavities.[40,41] These gradients may result in relatively high acoustic streaming velocities, i.e., steady fluid motion induced by the USW field in the absence of cavitating agents.[42] Such devices are therefore not well suited to the study of cavitation induced bioeffects, since, for example, strongly resonating acoustofluidic systems can themselves generate intracellular delivery of pharmaceutical compounds, due to the associated high streaming velocities.[27]

C. Challenges

A combination of microscopy, high speed imaging, acoustic monitoring, and chemical and biological assays is required in order to study the interactions between US-RAs and tissue. An ideal system should therefore:

(i)   Provide a well defined and spatially uniform acoustic pressure field to provide consistent exposure conditions across a sample.
(ii)   Minimise secondary acoustic effects, i.e., streaming and/or heating, to enable decoupling of the effects of US from those mediated by US-RAs.
(iii)   Operate at US frequencies of therapeutic relevance, i.e., in the range 0.3–2 MHz.
(iv)   Mimic the dimensional confinement typical of physiological microenvironments and physiologically relevant flow conditions.
(v)   Be compatible with small working-distance and/or high-magnification microscope objectives and high intensity illumination to facilitate high speed imaging of microbubble dynamics and/or fluorescence microscopy *in situ*.
(vi)   Enable simultaneous monitoring of acoustic emissions.
(vii)   Allow biological material to be maintained in a viable condition for sufficient time periods.
(viii) Enable convenient injection and extraction of material for analysis.
(ix)   Be simple to operate, economical, and reusable.

We have attempted to develop an acoustofluidic device to meet these requirements. The design is based on a thin-reflector resonator configuration,[27,43] which has been adapted to achieve a uniform acoustic pressure field in the direction of US propagation, at ultrasound frequencies suitable for transmission through both hard (0.5 MHz) and soft tissues (1 MHz).

In Secs. II and III, the construction of the device, characterisation of the acoustic field, and thermal properties are presented. In Sec. IV, the utility of the device in characterising the behaviour of US-RAs both optically (using a high-magnification objective) and acoustically (using a polyvinylidene fluoride film) is demonstrated. A method for mapping the fluid velocity produced by cavitation microstreaming using particle streak velocimetry (PSV) is described. Finally, a demonstration of the device in observing bubble-cell interaction, quantifying the effects upon cell membrane integrity, and determining the efficiency of microbubble-mediated cell sonoporation is presented.

II. DEVICE DESIGN AND FABRICATION

The microfluidic layered acoustic resonator (μLAR) devices used in this study consist of the following layers: i. a single piezoelectric element, ii. a ceramic carrier, iii. a fluid cavity, and iv. a glass reflector (Fig. 1). Each μLAR is designed to be operated at the first thickness-mode resonant frequency of its layered structure and has an acoustic pressure minimum located at the reflector-air boundary. This is in contrast to commonly employed half-wave and quarter-wave resonators, which typically have acoustic pressure nodes within their fluid cavities.[44]

Thus, whilst half-wave resonators may trap particles at the midplane of the fluid cavity and quarter-wave resonators may manipulate particles nearby a boundary of the fluid cavity, in the μLAR configuration presented here the acoustic pressure gradient is minimised in the direction of ultrasound propagation across the fluid layer. The reflecting layer of the μLAR is much smaller than the wavelength of sound in the layered structure, thus potentially allowing for a more uniform field in the direction of ultrasound propagation at the cost of reflecting less acoustic energy into the fluid cavity. This trade-off nonetheless results in acoustic pressures and field gradients that are relevant for ultrasound mediated bioeffects. It should be noted that the terms "reflector" and "carrier," which will be retained for the sake of consistency with the literature, do not strictly describe the function of these respective layers in the μLAR configurations presented herein. μLARs were thus designed as thin-reflector layered acoustic resonators, the advantages and disadvantages of which are discussed in Secs. II A–II D.

A. The piezoelectric transducer

Two μLAR devices were designed to efficiently resonate at two therapeutically relevant ultrasound frequencies: 0.5 and 1 MHz. Commercially available 1 mm and 2 mm thick PZT-4 elements (Meggitt, UK) were employed to achieve the required thickness-mode resonances for the 1 MHz and 0.5 MHz μLAR designs, respectively. The adhesive used to permanently bond the piezoelectric transducer to the machinable ceramic carrier layer (Macor, Corning Inc.) was a two-part epoxy chosen to provide efficient acoustic coupling and to prevent formation of air voids at the interface between the transducer and the carrier. The one and two dimensional modelling performed in the design of the devices is included in the supplementary material (S2).

B. The carrier

Macor was selected as the carrier layer material because it provides excellent coupling and transmission of the ultrasound field with the fluid layer owing to its acoustic impedance (14 MRayl). It has a speed of sound (c) of 2520 m/s and a density (ρ) of 5631 kg/m^3, in comparison with PZT-4 (c = 4530 m/s, ρ = 7600 kg/m^3). Macor is preferable to other ceramics because it can be machined using ordinary metalworking tools to 13 μm tolerances and can be inexpensively obtained at custom thicknesses and low quantities (in the present work, the Macor was from Ceramic Substrates and Components Ltd.). Moreover, it is a good thermal and electrical insulator, has a negligible thermal expansion coefficient, minimal outgassing, and porosity (making it well suited to biological work), and is compatible with piezoelectric transducers, and for use with gas-filled agents.
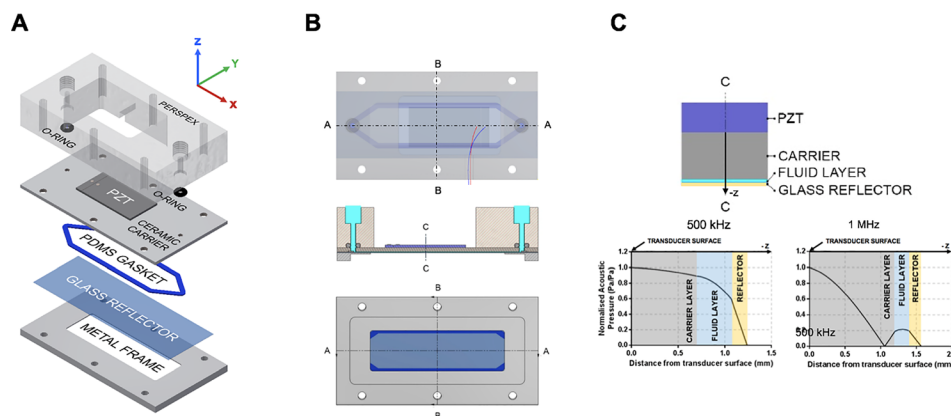

FIG. 1. Design of a μLAR device. (a) Expanded view of the layered acoustic resonator including, top to bottom: (i) Perspex® manifold, (ii) o-rings, (iii) piezoceramic element coupled to the Macor carrier layer, (iv) polydimethylsiloxane (PDMS) gasket that forms the channel geometry, (v) glass coverslip, and (vi) aluminium frame. (b) Schematic drawing of the assembled acoustofluidic device, showing relative layer thicknesses and cut-view in C-C and A-A planes. (c) Predicted pressure profiles within the device.

The μLAR is fully compatible with fluorescence and reflection microscopy, which are sufficient for most biophysical investigations. One drawback of Macor is that it is optically opaque, rendering the μLAR incompatible with brightfield microscopy.[31] However, the Macor carrier can be sputter-coated with a nanoscopic layer of gold or aluminium to make it highly reflective. We employed this approach to enable imaging of microbubbles in the μLAR without fluorescence labelling, as is often necessary for high-speed imaging studies (described below) or for preserving fluorescence bandwidth.

C. The thin reflector

The thin-reflector design of the μLAR has several practical motivations. First and foremost, a thin reflecting layer allows for better optical accessibility. For both μLAR designs presented herein, a widely commercially available glass coverslip was chosen as the reflector. Specifically, a #1.5 coverslip with 170 μm thickness was selected for compatibility with high-magnification microscopy and oil-immersion objectives. In addition to optimal optical characteristics, glass coverslips can be sterilized, provide a standard substrate for cellular adhesion and growth, are inexpensive, do not need to be altered or machined for use in a μLAR device, are disposable and/or reusable, and have acceptable thickness variations across batches for use in μLARs (±10%).

D. Construction

For the 1 MHz device, a $30 \times 13 \times 1$ mm^3 piezoelectric element (PZT-4, Meggitt PLC, UK) was acoustically coupled with a machinable ceramic layer using a thin film of epoxy resin (RX771C/NC, Robnor Resins Ltd, UK) cured at 30 °C for 24 h. To fabricate the 0.5 MHz device, a $30 \times 13 \times 2$ mm^3 PZT-4 piezoceramic element (Meggitt PLC, UK) was used. A fluid layer surrounded by a recess was milled in the ceramic layer. A polydimethylsiloxane (PDMS) gasket (Sylgard 184® Dow Corning Corporation, USA) was placed within the recess and was formed by mixing previously degassed PDMS precursor and curing agent (10:1 w/w), followed by a 1 h curing step at 90 °C. The reflector layer consists of a $75 \times 25 \times 0.17$ mm^3 glass slide (Logitech Ltd., Scotland). The layered device was held in place with a Perspex® block fitted with flat-bottom thread fluidic connectors ($^1/_4$ in.-28) to deliver fluid suspensions of US-RAs to the fluid layer of the device. An aluminium frame with optical access was used to secure the device layers simultaneously, allowing for microscopy. Table I summarises the geometric features and materials of the two devices. A schematic of the device is shown in Fig. 1, and full Computer Aided Design (CAD) drawings can be found in the supplementary material (S1).

III. DEVICE CHARACTERISATION

A. Acoustic pressure

Therapeutically relevant pressures for sonoporation typically range from 0.15 to 0.5 MPa,[45] with *in vitro* studies reporting membrane poration at acoustic pressures as low as 0.08 MPa.[46] Acoustic pressure also influences the lifetime of contrast agents both *in vitro* and *in vivo*. Microbubbles can exist and oscillate up to 20 000 cycles at 1 MHz under low acoustic pressures (0.1 MPa), but their lifetime is significantly decreased at higher pressures (100 cycles at 0.4 MPa[47]) and/or lower frequencies. Experimental values of the acoustic pressure in the μLARs for different driving transducer voltages were determined by inserting a fibre-optic hydrophone into the fluid layer of the devices. Three independent measurements were performed in the 0–77 V range to yield the input voltage-acoustic pressure curve shown in Figs. 2(a) and 2(b). The chamber was filled with deionised water, the fibre-optic tip was inserted through a 0.5 mm hole in the reflector layer, and a pressure ramp was measured at varying driving voltages. A positive correlation between the acoustic pressure and input voltage was observed, with acoustic pressure peaks of 0.25 MPa Peak Rarefactional Pressure (PRFP) for the 1 MHz device, and 0.4 MPa for the 0.5 MHz device. It should be noted that other, less invasive methods for measuring acoustic pressure in microscale USW fields have been reported, such as the "drop

TABLE I. Geometric and material properties of the constitutive layers for both the 0.5 MHz and the 1 MHz devices. The US wavelengths corresponding to 0.5 MHz and 1 MHz were calculated as 2.96 mm and 1.48 mm, respectively. The thicknesses refer to the layers shown in Fig. 1(b).

	Layer	Material	Thickness (μm)	Thickness/λ	Density (kg/m^3)	Speed of sound (m/s)
1 MHz device	Transducer	PZT-4	1000	0.676	7600	4530
	Glue layer	Epoxy	10	0.006	2156	2640
	Matching layer	Macor®	1200	0.811	5631	2520
	Fluid layer	Water	200	0.135	1000	1482
	Reflector	Glass	170	0.115	2200	5710
0.5 MHz device	Transducer	PZT-4	2000	0.676	7600	4530
	Glue layer	Epoxy	10	0.003	2156	2640
	Matching layer	Macor®	700	0.236	5631	2520
	Fluid layer	Water	370	0.125	1000	1482
	Reflector	Glass	170	0.057	2200	5710

voltage" technique.[27,48] These methods, however, usually require efficient particle manipulation to the nodes of the USW and therefore are not applicable to characterizing acoustofluidic devices with weak acoustic pressure gradients across their fluid cavities.

B. Transducer temperature

Biological cells are typically very sensitive to variations in temperature, and in a small fluid volume, the heating produced by the ultrasound transducer cannot be ignored. The temperature response of the piezoelectric element was monitored during continuous excitation using an infrared thermal imager (Monition Ltd. UK). The transducers were driven at 76.6 V for 15 min and left to cool down for a further 15 min. Figure S7 in the supplementary material shows the temperature over the transducer surface as a function of time, indicating a sharp increase in temperature ($\Delta 1.5\,^\circ$C for the 500 kHz device, $\Delta 1.0\,^\circ$C for the 1 MHz) in the first 3 min. This difference, however, will have little influence on the temperature of the fluid layer, given the low thermal conductivity of MACOR (1.5 W/m/K)[49] and of the glue layer. Furthermore, sonoporation studies do not typically involve long exposures (<10 min) to continuous wave ultrasound. This makes μLAR devices suitable for investigating the effects of ultrasound and US-RAs on target biological cells, by minimising secondary thermal effects caused by heating from the ultrasound source.

C. Resonance frequency verification

The resonance frequencies of the devices were verified experimentally using an impedance spectral analyser (C60, Cypher Instruments LLC) and found to be 513 kHz and 908 kHz for the
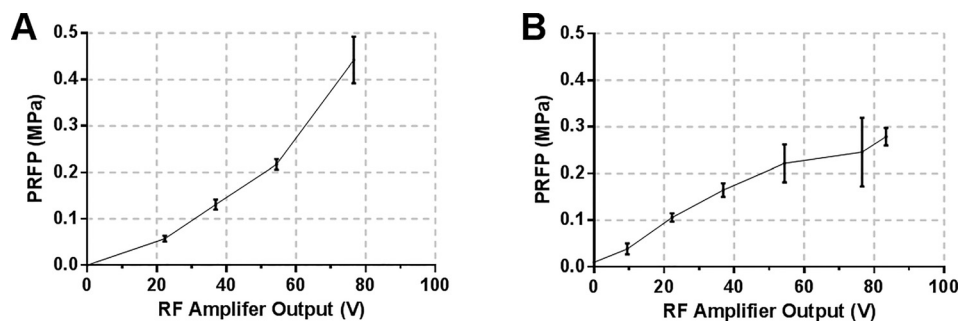

FIG. 2. Ultrasound pressure calibration. Peak Rarefactional Pressure (PRFP) as a function of transducer driving voltage for the (a) 0.5 MHz device and (b) 1 MHz device. Pressure was determined experimentally using a fibre-optic hydrophone.

0.5 MHz and 1 MHz devices, respectively. The impedance analysis was performed in both air- and water-filled conditions, in order to clearly identify the first thickness resonant frequency of the fluid-filled layered structure. The discrepancies between experimental measurements and 1D model predictions may be caused by fabrication tolerances, tightness of the assembly, and lateral modes of vibration. The device was consistently operated at the experimentally determined resonant frequencies. Impedance spectra for both devices are included in the supplementary material (S5).

IV. MEASUREMENTS

As indicated in the introduction, it is desirable to be able to perform simultaneous measurements of microbubble dynamics, fluid motion, acoustic emissions, and cellular response within the same device in order to probe the mechanisms underlying bubble-cell interactions. Sections IV A–IV D describe how these measurements can be performed within the μLAR and present sample data for each.

A. Imaging of microbubble dynamics

Characterising the dynamic response of microbubbles to ultrasound excitation is essential in determining the mechanism(s) underpinning interactions between cells and US-RAs. Bubble oscillations may be highly non-linear, even at moderate ultrasound pressures, requiring extremely high imaging frame rates (>5 MHz) and consequently specialised cameras and illumination sources.[19] To be compatible with these systems, the μLAR must provide sufficient optical access to the region of interest in terms of both the dimensions of the chamber and optical transparency of the upper layers. To confirm this, oscillations of SonoVue$^\circledR$ (Bracco, Switzerland) microbubbles in the 500 kHz μLAR were recorded using the Brandaris 128 high-speed camera[19,50] in a series of 128 frame acquisitions recorded at 6×10^6 frames per second (6 Mfps) at 10X magnification. The setup for Brandaris-128 experiments is shown in Fig. 3(a). To facilitate visualization of microbubble dynamics at high frame rates in the μLAR, the Macor carrier layer was gold sputtered for 240 s at approximately 1 Å/s, using a Cressington 108 sputter coater. The μLAR was positioned with the glass-reflector facing upwards toward the microscope objective of the Brandaris-128. Illumination was achieved using a continuous wave (CW) light emitting diode (LED) source (KL2500 LED, Schott) and a Xenon strobe flash.

A segment of the radius-time curve for an inertially-collapsing SonoVue$^\circledR$ microbubble extracted from the camera footage can be seen in Fig. 3(b).
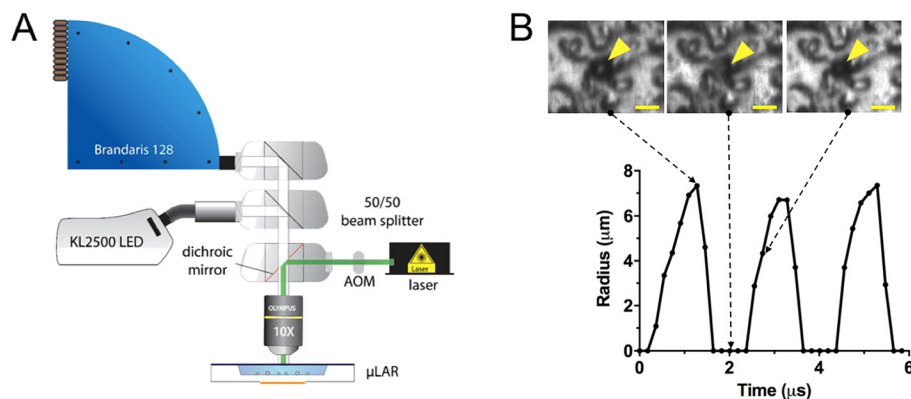

FIG. 3. Capturing microbubble dynamics in the μLAR with the Brandaris-128 high-speed camera. A) Schematic of the experimental setup. (b) Radius-time curve from an oscillating SonoVue$^\circledR$ microbubble under ultrasound exposure (511 kHz and ~145 kPa PRFP from 40 V driving voltage) as captured by the Brandaris-128 high speed camera at 6×10^6 frames per second. Note that when the microbubble was too small to image, the radius was entered as 0 μm on the radius-time curve.

B. Quantification of cavitation microstreaming velocities

Microstreaming has been hypothesized to play a major role in ultrasound-mediated drug delivery.[37,51,52] Shear stress and shear stress gradients have been associated with increased permeability,[53,54] and may play a role in, e.g., ultrasound-mediated blood-brain barrier opening[55,56] as well as in sonoporation.[57] It is therefore important to be able to visualise and quantify the flow field within the device so that correlation to cellular response can be investigated.

1. Particle streak velocimetry (PSV)

There are multiple techniques for flow quantification, including particle image velocimetry (PIV), ultra-high-speed particle tracking velocimetry (PTV),[58] or astigmatism particle tracking velocimetry (APTV).[59,60] For the purposes of illustration, the comparatively simple technique of PSV was used here, but all of these methods can be employed with the μLAR. A suitable flow tracer, typically a suspension of fluorescent particles, is injected into the region of interest. The motion of the tracer is then imaged over a series of frames. If the image exposure time is longer than the time required for a tracer particle to travel the physical pixel size of the images, a streak is produced in the image capturing the path of the particle. The average velocity of the tracer particle during the exposure time is the measured arc-length of the streak in the image divided by the exposure time. Thus with PSV, rapid changes in the flow field can be quantified from a single streak image. A MATLAB PSV image analysis routine for determining particle streak velocities from standard fluorescence microscopy videos is included in the Supplementary Material together with an uncertainty analysis.

2. Microstreaming from different US-RAs

Streak images were obtained by co-injection of a solution containing $2\,\mu$m diameter fluorescent beads used as flow tracers (Sigma Aldrich, used at 1:1000 dilution) with one of 3 different US-RAs: SonoVue® microbubbles, gas-trapping polymeric cups, and phase-shift droplets. Preparation of these cavitation agents is detailed in the supplementary material (S9–S11). In the 1 MHz μLAR, SonoVue® microbubbles [Figs. 4(a) and 4(b)], gas-trapping polymeric cups [Figs. 4(c) and 4(d)], and phase-shift droplets [Figs. 4(e) and 4(f)] all produced cavitation microstreaming flows under ultrasound exposure (videos are included in the supplementary material). At 1 MHz, a dipole microstreaming pattern with the microbubble located at the centre of the dipole was most commonly observed. Streaming patterns involving multiple microbubbles were also observed that were qualitatively similar to those described by Ooi *et al.* for larger bubbles.[60] The highest recorded microstreaming velocities, as determined by PSV, were on the order of $1000\,\mu$m/s and microstreaming patterns were found to produce velocities greater than $100\,\mu$m/s at a distance of more than 1 mm from the cavitating microbubble. This corresponds to an average wall shear stress from microstreaming on the order of 1 mPa which agrees well with the study by Collis *et al.*[16] on shear stress from cavitation microstreaming.

C. Monitoring of acoustic emissions

Acoustic emissions monitoring provides a means of classifying and quantifying cavitation activity non-invasively during ultrasound-mediated therapy with clinically relevant spatial and temporal resolution.[61,62] It is thus of interest for any *in vitro* experiment investigating cavitation to simultaneously (passively) monitor acoustic emissions. Acoustic emissions from SonoVue® (Bracco, Switzerland) microbubbles, which give rise to both non-inertial and inertial cavitation activity, and gas-trapping polymeric cups, which only cavitate inertially, were monitored using a commercially available electrically-insulated $28\,\mu$m thick polyvinylidene difluoride (PVDF) film sensor (SDT1–028K, Measurement Specialties) while exposed to ultrasound in the 500 kHz μLAR device. The sensor was externally coupled with ultrasound gel to the glass reflecting layer and held in place using the aluminium frame of the 500 kHz μLAR device. The voltage
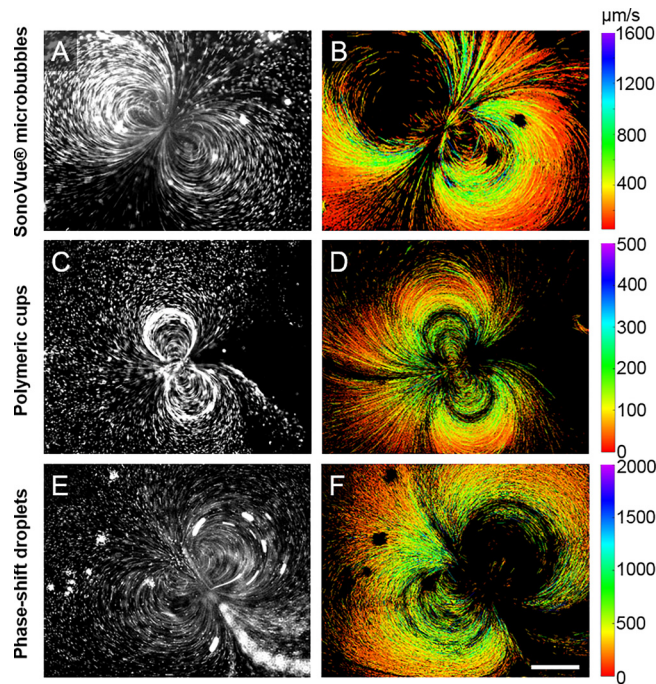
FIG. 4. Streak velocimetry performed on videos of fluorescent tracer beads moving in cavitation microstreaming flows induced by SonoVue® microbubbles (top), gas-trapping sub-micron polymeric cups (middle), and phase-shift droplets (bottom) under ultrasound exposure inside the μLAR (511 kHz and ~145 kPa PRFP from 40 V driving voltage). Figures show a brightness and contrast enhanced still from the videos analysed (left), and a pseudo-coloured composite of the headless velocity vectors for each streak analysed in the respective video (right). Colour bars are in μm/s. Scale bar = 350 μm.

output from the PVDF sensor was amplified with 5× gain (SR445A, Stanford Research Systems) before being recorded with an oscilloscope (Waverunner 62 X*i*, Teledyne LeCroy).

It was found that the PVDF film sensor externally-coupled to the 500 kHz μLAR device was capable of detecting harmonic, ultra-harmonic, and broadband emissions from clinical ultrasound contrast agent SonoVue® microbubbles (Bracco, Switzerland) and polymeric nanocups (see Fig. 5). The acoustic emission results and fibre-optic hydrophone pressure measurements obtained from the acoustofluidic device are in good agreement with the acoustic emissions thresholds reported in the literature[18] for SonoVue® at 500 kHz and obtained using a conventional water-tank apparatus. Harmonic emissions at low ultrasound pressure, followed by widening of harmonic peaks and leakage of energy into ultra-harmonics as the ultrasound pressure increased, and finally broadband emissions at high ultrasound pressures were observed (Fig. 5).

Acoustic emissions from gas-trapping polymeric cups are decidedly different. Notably, the acoustic emission data from polymeric cups in the 500 kHz μLAR agree with the previously described[5] broadband emissions threshold for these cavitation nuclei. Upon increasing the acoustic pressure, the polymeric cups exhibit a step-change from producing only modest acoustic emissions to producing substantial broadband noise. This threshold is hypothesised to be associated with the pressure required to elicit a bubble from the cup, which is coincident with the inertial cavitation threshold.[63]

D. Monitoring of biological effects

Fluorescence microscopy for visualising and quantifying interactions between US-RAs and cells remains an indispensable modality for understanding the interplay between such experimental parameters and the resultant biological effects. It has been used to quantify changes in intracellular calcium,[64] reactive oxygen species generation,[65] actin cytoskeleton integrity,[66] membrane lipid ordering,[14] and vesicular activity,[15] among others.[13,24] The μLAR devices presented herein enable simultaneous control of ultrasound excitation and fluorescence microscopy
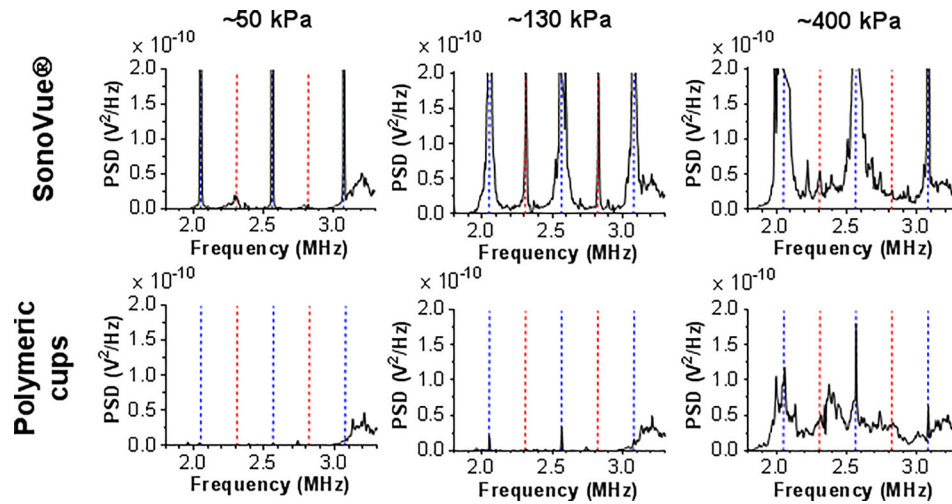
FIG. 5. Acoustic emissions of SonoVue® and polymeric cups exposed to 511 kHz ultrasound in a μLAR device, as detected by an externally coupled PVDF film sensor. The power spectral density is shown following background subtraction using the acoustic emissions of a control sample (no cavitation nuclei). The blue dashed lines indicate the harmonic frequencies. The red dashed lines indicate the ultra-harmonic frequencies. The peak rarefactional pressure (PRFP) of the ultrasound is indicated in the figure.

without the need for the more complex setups often employed to conduct such mechanistic investigations. In addition to compatibility with high magnification fluorescence microscopy, a key feature of the μLAR design is the ability to visualize during ultrasound exposure enabling the quantification of dynamic processes whether mechanical (e.g., microbubble oscillations, microstreaming flow fields, microbubble/cell membrane penetration), chemical (e.g., reactive oxygen species generation, lipid shedding/exchange), thermal (e.g., using thermo-sensitive dyes), or biological (e.g., subcellular response, drug uptake, vesicular transport). Protocols for using μLAR devices with living cells and fluorescence microscopy are detailed in the supplementary material (S12). Examples of the utility of the μLAR for conducting *in vitro* experiments with cells and microbubbles are illustrated in Fig. 6.

1. Bubble-cell interaction

Figure 6(a) shows the direct interaction between a fluorescent microbubble and a fluorescently-labelled cell plasma membrane following exposure to CW ultrasound at 1 MHz, 210 kPa for 60 s. This demonstrates the ability to visualize living cells and microbubbles *in situ* within the μLAR at high spatial resolution during and after ultrasound exposure.

2. Quantification of cell membrane properties

The μLAR also facilitates monitoring of cellular response to ultrasound exposure using appropriate fluorescent probes and quantitative microscopy techniques. Figure 6(b) shows cells labelled with a polarity-sensitive dye, c-Laurdan, used to determine membrane lipid packing as an indicator of permeability. The cells were imaged at 30 different emission wavelengths to quantify the spectral shift of c-Laurdan in response to ultrasound and microbubbles exposure. This technique was employed recently to quantify changes in the lipid packing of membranes resulting from the transfer of phospholipids from microbubble shell to cell plasma membranes,[14] in the 1 MHz μLAR.

3. Quantification of intracellular delivery

Targeted delivery of therapeutics is a key application area of biomedical ultrasound research. One way to achieve ultrasound and cavitation-enhanced delivery of therapeutics is by cavitation-mediated permeabilisation of the cell membrane, often referred to as sonoporation. In
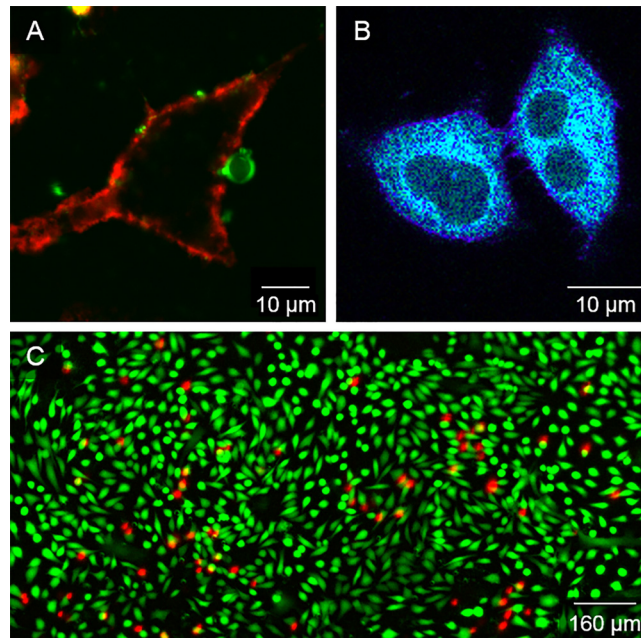
FIG. 6. Demonstration of microscopy with the μLAR device and biological cells. (a) A-549 cell plasma membrane labelled with CellMask[TM] (red) and a fluorescent microbubble labelled with DiI (green) adhering to the cell membrane. (b) A-549 cells labelled with polarity-sensitive dye c-Laurdan, used to determine membrane physical properties such as lipid packing. Image taken following ultrasound and microbubble exposure. Purple/blue regions indicate areas with higher/lower lipid bilayer hydration, while the dark areas within the cells indicate the cell nuclei. (c) Sonoporation assay using cell-impermeant propidium iodide (red) to indicate permeability or cell death, and calcein-AM (green) to indicate cell viability in MDCK cells exposed to ultrasound (511 kHz at ∼145 kPa PRFP from 40 V driving voltage, 10 ms bursts at 1% duty cycle for 60 s) and microbubbles. Sonoporated cells are indicated by simultaneous propidium iodide and calcein-AM fluorescence. The percentage of sonoporated cells was quantified using a purpose-written MATLAB script and determined to be 5.5%.

a third example experiment with the μLAR device, Madin-Darby Canine Kidney (MDCK) cells were sonoporated following ultrasound and microbubble exposure in the 500 kHz μLAR device. Figure 6(c) shows the results of a typical fluorescence sonoporation evaluation using cell-impermeant propidium iodide (red) to indicate permeability or cell death, Calcein-AM (green) to indicate cell viability, and co-localized propidium iodide and Calcein-AM fluorescence to indicate successful sonoporation. The ultrasound frequency and pressure used for sonoporation (511 kHz and ∼145 kPa) were also employed in the assessment of microbubble cavitation dynamics in the μLAR with the Brandaris-128 high-speed camera (Fig. 3), and in the assessment of cavitation microstreaming flow fields from microbubbles under ultrasound exposure (Fig. 4). It follows that the 5.5% sonoporation observed, coincided with millimetre-scale cavitation microstreaming events, and stable, non-linear microbubble cavitation dynamics associated with the generation of harmonic and ultraharmonic acoustic emissions.

By reporting sonoporation results with corresponding characterizations of cavitation dynamics, microstreaming flow fields, and acoustic emissions, discrepancies in the field with regard to the experimental parameters (e.g., driving frequency, pulse repetition frequency (PRF), pulse length, total exposure time, dissolved gas concentration, cavitation agent) that result in sonoporation and the associated mechanisms can be addressed.[10,67,68] It is known, for instance, that inertial cavitation, which correlates with cell death, is associated with broadband acoustic emissions,[7,12,69,70] although acoustic emissions are often not reported in sonoporation experiments. Furthermore, cavitation microstreaming is often cited[10,46,51,52,67,71] as a principle mechanism of sonoporation owing to the high fluid shear stresses generated close to the microbubble,[57] and yet, cavitation microstreaming flow field measurements have never been reported in sonoporation experiments with adherent cells. Employing the μLAR for the concurrent measurement of acoustic emissions, cavitation microstreaming, and sonoporation efficiency, for instance, may

also aid *in vivo* translation, where monitoring of acoustic emissions can be achieved, but correlations with fluid flows, cavitation dynamics, and permeabilization are not well-established.

V. LIMITATIONS AND FUTURE PERSPECTIVES

In its current configuration, the μLAR utilises a rigid glass surface as a substrate for biological cells. The mechanical properties of physical boundaries can impact on microbubble cavitation dynamics and the associated microstreaming patterns; but they will also have an effect on the behaviour of cells either in the presence or in the absence of mechanical stimuli. Future work will investigate how these properties may influence ultrasound-mediated bioeffects. Reflector layers with different mechanical properties could be employed to mimic different soft and hard target tissues. For instance, Glynne-Jones *et al.*[43] reported on a thin-reflector resonator comprising a cellulose acetate reflector layer, designed for manipulation of microparticles towards a surface. In order to mimic a softer substrate (which is relevant to many *in-vivo* conditions), the glass surface could also be coated using an acoustically- and optically-transparent hydrogel. For instance, the acoustical properties of biocompatible materials—including hydrogels—with different stiffness have been systematically investigated in a recent study by Cafarelli *et al.*[72] Cells could be potentially seeded within the hydrogel layer to also generate a three-dimensional microenvironment, as opposed to a two-dimensional monolayer of cells as reported in the present study.

In this study, we reported on acoustic pressures in the range 0–0.4 and 0–0.3 MPa for the 0.5 and the 1 MHz resonators, respectively. It may however be desirable to generate a wider range of acoustic pressures, to replicate different acoustic stimulation regimes and therapeutic applications of ultrasound. In order to minimise undesired increase in transducer temperature at the higher driving voltages, the use of pulsed wave may be preferable. A temperature controlled system (based on Peltier elements) could also be integrated with the device, as reported by Ohlin *et al.*[40] for an acoustofluidic device intended for cell levitation and manipulation at 1 MPa acoustic pressure.

Again, in the experiments reported here, flow was only utilised to enable changes of medium and for injection of tracer particles and fluorescent dyes. It should be noted, however, that μLAR could also act as a flow cell, for exposure of biological cells to physiologically relevant fluid shear stress levels. The aspect ratio of the fluid layer and its tapered inlet/outlet sections are designed to generate a relatively uniform shear stress field over the reflector surface. Flow perfusion may also be beneficial if medium replenishment is needed, for long-term acoustic stimulation experiments. In addition, particle trapping and size-selective sorting of microscale particles have been achieved by manipulating cavitation microstreaming patterns in the presence of a pressure-driven background flow.[73] The μLAR device concept could be employed to further develop and characterize this technique.

VI. CONCLUSIONS

Ultrasound, in particular in combination with US-RAs, has shown potential for inducing therapeutically relevant effects on cells and tissues, with application in the treatment of malignant and non-malignant diseases. A more comprehensive understanding of their interaction with biological systems, however, requires the ability to generate acoustic fields within physical domains that are accessible by high-resolution analytical and optical instruments. This is difficult to achieve using water-tank based equipment that is commonly employed in biomedical ultrasound laboratories.

In order to overcome this limitation, we presented the design, fabrication, and experimental characterisation of acoustofluidic resonators (μLARs) suitable for investigating the acoustic behaviour of US-RAs and their interaction with biological cells. The devices are based on a thin-reflector resonator configuration, adapted to minimise pressure gradients in the direction of ultrasound propagation; as well as thermal and other secondary effects of ultrasound, e.g., acoustic streaming, allowing for the discrimination of the effects of US alone from those of US-RAs.

In the paper, we demonstrated the generation of ultrasound fields at therapeutically relevant acoustic pressures and frequencies; compatibility of the devices with ultra high speed imaging for monitoring microbubble dynamics; the integration of transducers for simultaneously recording acoustic emissions; quantification of the microstreaming flows produced by different US-RAs using particle streak velocimetry; and observation and quantification of ultrasound/cavitation mediated changes in cell membrane permeability and intracellular delivery using fluorescence microscopy.

SUPPLEMENTARY MATERIAL

See supplementary material for detailed specifications of the device, implementation of particle streak velocimetry and details of the cell culture and cavitation agent preparation.

ACKNOWLEDGMENTS

[1] A. K. W. Wood and C. M. Sehgal, Ultrasound Med. Biol. **41**, 905 (2015).

[2] M. Aryal, C. D. Arvanitis, P. M. Alexander, and N. McDannold, Adv. Drug Delivery Rev. **72**, 94 (2014).

[3] A. Azagury, L. Khoury, G. Enden, and J. Kost, Adv. Drug Delivery Rev. **72**, 127 (2014).

[4] K. Ferrara, R. Pollard, and M. Borden, Annu. Rev. Biomed. Eng. **9**, 415 (2007).

[5] J. J. Kwan, R. Myers, C. M. Coviello, S. M. Graham, A. R. Shah, E. Stride, R. C. Carlisle, and C. C. Coussios, Small **11**, 5305 (2015).

[6] S. R. Sirsi and M. A. Borden, Adv. Drug Delivery Rev. **72**, 3 (2014).

[7] J. Y. Lee, D. Carugo, C. Crake, J. Owen, M. De Saint Victor, A. Seth, C. Coussios, and E. Stride, Adv. Mater. **27**, 5484 (2015).

[8] C. Crake, J. Owen, S. Smart, C. Coviello, C. C. Coussios, R. Carlisle, and E. Stride, Ultrasound Med. Biol. **42**, 3022 (2016).

[9] G. Korpanty, J. G. Carbon, P. A. Grayburn, J. B. Fleming, and R. A. Brekken, Clin. Cancer Res. **13**, 323 (2007).

[10] I. Lentacker, I. De Cock, R. Deckers, S. C. De Smedt, and C. T. W. Moonen, Adv. Drug Delivery Rev. **72**, 49 (2014).

[11] A. van Wamel, K. Kooiman, M. Harteveld, M. Emmer, F. J. ten Cate, M. Versluis, and N. de Jong, J. Controlled Release **112**, 149 (2006).

[12] N. Kudo, K. Okada, and K. Yamamoto, Biophys. J. **96**, 4866 (2009).

[13] I. De Cock, G. Lajoinie, M. Versluis, S. C. De Smedt, and I. Lentacker, Biomaterials **83**, 294 (2016).

[14] D. Carugo, M. Aron, E. Sezgin, J. Bernardino de la Serna, M. K. Kuimova, C. Eggeling, and E. Stride, Biomaterials **113**, 105 (2017).

[15] L. J. M. Juffermans, A. van Dijk, C. A. M. Jongenelen, B. Drukarch, A. Reijerkerk, H. E. de Vries, O. Kamp, and R. J. P. Musters, Ultrasound Med. Biol. **35**, 1917 (2009).

[16] J. Collis, R. Manasseh, P. Liovic, P. Tho, A. Ooi, K. Petkovic-Duran, and Y. Zhu, Ultrasonics **50**, 273 (2010).

[17] L. Wang, J. Tu, X.-S. Guo, D. Xu, and D. Zhang, Chin. Phys. B **23**, 124302 (2014).

[18] C. D. Arvanitis, M. Bazan-Peregrino, B. Rifai, L. W. Seymour, and C. C. Coussios, Ultrasound Med. Biol. **37**, 1838 (2011).

[19] G. Lajoinie, I. De Cock, C. C. Coussios, I. Lentacker, S. Le Gac, E. Stride, and M. Versluis, Biomicrofluidics **10**, 11501 (2016).

[20] G. Lukinavicius, K. Umezawa, N. Olivier, A. Honigmann, G. Yang, T. Plass, V. Mueller, L. Reymond, I. R. Corrêa, Z.-G. Luo, C. Schultz, E. A. Lemke, P. Heppenstall, C. Eggeling, S. Manley, and K. Johnsson, Nat. Chem. **5**, 132 (2013).

[21] C. Di Rienzo, E. Gratton, F. Beltram, F. Cardarelli, C. Di Rienzo, E. Gratton, F. Beltram, C. Di Rienzo, E. Gratton, F. Beltram, and F. Cardarelli, Proc. Natl. Acad. Sci. U. S. A. **110**, 12307 (2013).

[22] I. López-Duarte, T. T. Vu, M. A. Izquierdo, J. A. Bull, and M. K. Kuimova, Chem. Commun. (Cambridge) **50**, 5282 (2014).

[23] D. M. Owen, C. Rentero, A. Magenau, A. Abu-Siniyeh, and K. Gaus, Nat. Protoc. **7**, 24 (2012).

[24] I. De Cock, E. Zagato, K. Braeckmans, Y. Luan, N. de Jong, S. C. De Smedt, and I. Lentacker, J. Controlled Release **197**, 20 (2015).

[25] D. Carugo, J. Owen, C. Crake, J. Y. Lee, and E. Stride, Ultrasound Med. Biol. **41**, 1927 (2015).

[26] P. Marmottant, J. P. Raven, H. Gardeniers, J. G. Bomer, and S. Hilgenfeldt, J. Fluid Mech. **568**, 109 (2006).

[27] D. Carugo, D. N. Ankrett, P. Glynne-Jones, L. Capretto, R. J. Boltryk, X. Zhang, P. A. Townsend, and M. Hill, Biomicrofluidics **5**, 44108 (2011).

[28] L. Meng, F. Cai, P. Jiang, Z. Deng, F. Li, L. Niu, Y. Chen, J. Wu, and H. Zheng, Appl. Phys. Lett. **104**, 073701 (2014).

[29] W. Longsine-Parker, H. Wang, C. Koo, J. Kim, B. Kim, A. Jayaraman, and A. Han, Lab Chip **13**, 2144 (2013).

[30]F. Yuan, G. Sankin, and P. Zhong, J. Acoust. Soc. Am. **130**, 3339 (2011).

[31]M. Wiklund, H. Brismar, and B. Önfelt, Lab Chip **12**, 3221 (2012).

[32]M. Evander and J. Nilsson, Lab Chip **12**, 4667 (2012).

[33]A. Lenshof, C. Magnusson, and T. Laurell, Lab Chip **12**, 1210 (2012).

[34]A. Ozcelik, D. Ahmed, Y. Xie, N. Nama, Z. Qu, A. A. Nawaz, and T. J. Huang, Anal. Chem. **86**, 5083 (2014).

[35]N. Bertin, T. Spelman, T. Combriat, H. Hue, O. Stéphan, E. Lauga, and M. Philippe, Lab Chip **17**, 1515 (2017).

[36]S. Orbay, A. Ozcelik, J. Lata, M. Kaynak, M. Wu, and T. J. Huang, J. Micromech. Microeng. **27**, 15008 (2017).

[37]P. Marmottant and S. Hilgenfeldt, Nature **423**, 153 (2003).

[38]P. Marmottant and S. Hilgenfeldt, Proc. Natl. Acad. Sci. U. S. A. **101**, 9523 (2004).

[39]B. Rallabandi, C. Wang, and S. Hilgenfeldt, J. Fluid Mech. **739**, 57 (2014).

[40]M. Ohlin, I. Iranmanesh, A. E. Christakou, and M. Wiklund, Lab Chip **15**, 3341 (2015).

[41]M. Gedge and M. Hill, Lab Chip **12**, 2998 (2012).

[42]M. Wiklund, R. Green, and M. Ohlin, Lab Chip **12**, 2438 (2012).

[43]P. Glynne-Jones, R. J. Boltryk, M. Hill, N. R. Harris, and P. Baclet, J. Acoust. Soc. Am. **126**, EL75 (2009).

[44]D. Carugo, T. Octon, W. Messaoudi, A. L. Fisher, M. Carboni, N. R. Harris, M. Hill, and P. Glynne-Jones, Lab Chip **14**, 3830 (2014).

[45]T. van Rooij, I. Skachkov, I. Beekers, K. R. Lattwein, J. D. Voorneveld, T. J. A. Kokhuis, D. Bera, Y. Luan, A. F. W. van der Steen, N. de Jong, and K. Kooiman, J. Controlled Release **238**, 197 (2016).

[46]K. Kooiman, M. Foppen-Harteveld, A. F. W. Van Der Steen, and N. De Jong, J. Controlled Release **154**, 35 (2011).

[47]C. Mannaris and M. A. Averkiou, Ultrasound Med. Biol. **38**, 681 (2012).

[48]J. Lei, P. Glynne-Jones, and M. Hill, Lab Chip **13**, 2133 (2013).

[49]S. David, K. Sefiane, and L. Tadrist, Colloids Surf. A **298**, 108 (2007).

[50]C. T. Chin, C. Lancee, J. Borsboom, F. Mastik, M. E. Frijlink, N. De Jong, M. Versluis, and D. Lohse, Rev. Sci. Instrum. **74**, 5026 (2003).

[51]B. Helfield, X. Chen, S. C. Watkins, and F. S. Villanueva, Proc. Natl. Acad. Sci. 201606915 (2016).

[52]M. M. Forbes and W. D. O'Brien, J. Acoust. Soc. Am. **131**, 2723 (2012).

[53]Y. S. J. Li, J. H. Haga, and S. Chien, J. Biomech. **38**, 1949 (2005).

[54]J. M. Tarbell, Cardiovasc. Res. **87**, 320 (2010).

[55]W. Wiedemair, Ž. Tuković, H. Jasak, D. Poulikakos, and V. Kurtcuoglu, Phys. Med. Biol. **57**, 1019 (2012).

[56]N. Hosseinkhah, D. E. Goertz, and K. Hynynen, IEEE Trans. Biomed. Eng. **62**, 1293 (2015).

[57]A. A. Doinikov and A. Bouakaz, J. Acoust. Soc. Am. **128**, 11 (2010).

[58]B. Verhaagen, C. Boutsioukis, L. W. M. van der Sluis, and M. Versluis, J. Acoust. Soc. Am. **135**, 1717 (2014).

[59]R. Bolaños-Jiménez, M. Rossi, D. Fernandez Rivas, C. J. Kähler, and A. Marin, J. Fluid Mech. **820**, 529 (2017).

[60]A. Ooi, P. Tho, and R. Manasseh, J. Acoust. Soc. Am. **122**, 3051 (2007).

[61]C. C. Coussios, C. H. Farny, G. ter Haar, and R. A. Roy, Int. J. Hyperthermia **23**, 105 (2007).

[62]N. McDannold, N. Vykhodtseva, and K. Hynynen, Proc. - IEEE Ultrason. Symp. **2**, 1249 (2005).

[63]J. J. Kwan, S. Graham, R. Myers, R. Carlisle, E. Stride, and C. C. Coussios, Phys. Rev. E - Stat. Nonlinear, Soft Matter Phys. **92**, 023019 (2015).

[64]R. E. Kumon, M. Aehle, D. Sabens, P. Parikh, Y. W. Han, D. Kourennyi, and C. X. Deng, Ultrasound Med. Biol. **35**, 494 (2009).

[65]K. Kooiman, A. F. W. Van Der Steen, and N. De Jong, IEEE Trans. Ultrason. Ferroelectr. Freq. Control **60**, 1811 (2013).

[66]X. Chen, R. S. Leow, Y. Hu, J. M. F. Wan, and A. C. H. Yu, J. R. Soc. Interface **11**, 20140071 (2014).

[67]A. Delalande, S. Kotopoulis, M. Postema, P. Midoux, and C. Pichon, Gene **525**, 191 (2013).

[68]R. Karshafian, P. D. Bevan, R. Williams, S. Samac, and P. N. Burns, Ultrasound Med. Biol. **35**, 847 (2009).

[69]H. A. S. Kamimura, S. Wang, S. Y. Wu, M. E. Karakatsani, C. Acosta, A. A. O. Carneiro, and E. E. Konofagou, Phys. Med. Biol. **60**, 7695 (2015).

[70]Y. Hu, J. M. F. Wan, and A. C. H. Yu, Ultrasound Med. Biol. **39**, 2393 (2013).

[71]Z. Fan, R. E. Kumon, J. Park, and C. X. Deng, J. Controlled Release **142**, 31 (2010).

[72]A. Cafarelli, A. Verbeni, A. Poliziani, P. Dario, A. Menciassi, and L. Ricotti, Acta Biomater. **49**, 368 (2017).

[73]C. Wang, S. V. Jalikop, and S. Hilgenfeldt, Appl. Phys. Lett. **99**, 034101 (2011).